ROTOR BLADES AS CURVED, TWISTED AND TAPERED BEAM-LIKE STRUCTURES SUBJECTED TO LARGE DEFLECTIONS

G. Migliaccio[1] **and G. Ruta**[2]

[1] Civil and Industrial Engineering, University of Pisa
Largo Lucio Lazzarino 1, 56122, Pisa, Italy
e-mail: giovanni.migliaccio.it@gmail.com

[2] Structural and Geotechnical Engineering, University "La Sapienza" of Roma
Via Eudossiana 18, I-00184, Roma, Italy
e-mail: giuseppe.ruta@uniroma1.it

Abstract. *Non-prismatic beam-like structures are widespread in many engineering and science applications. Important examples include the rotor blades of wind turbines and helicopters. Their mechanical behaviour can be simulated using 3D beam models, which are computationally efficient, accurate and explicitly consider such structures' main geometric features, the large deflection of their reference centre-line and 3D warping of their transverse cross-sections. This paper proposes a mathematical model for such structures. A variational approach and the smallness of the warping and strain fields are exploited to obtain the model. Analytical and numerical results obtained with the proposed modelling approach are presented and compared to those from nonlinear 3D-FEM simulations.*

Keywords: non-prismatic, large deflection, cross-sections warping, taper effects.

1 INTRODUCTION

Many complex engineering components, such as the rotor blades of wind turbines and helicopters, are non-prismatic beam-like structures, which may be curved, twisted and tapered in their unstressed state and undergo large centre-line displacements, as well as in- and out-of-plane cross-sectional warping. Continuous efforts to better predict the mechanical behaviour of such structures are aimed at improving their performance in terms of structural efficiency and costs effectiveness [1-4]. At the same time, this offers the opportunity to address some very interesting, challenging problems in the field of continuum and solid mechanics.

Over the years many theories have been proposed for beam-like structures, from classical beam models for extension, twisting and bending [5], to formulations which include transverse shear deformation [6], to geometrically exact and asymptotic approaches, involving the research efforts of many investigators [7-13]. The available theories may be broadly grouped into engineering theories and mathematical ones. The former are generally based on ad-hoc corrections to simpler theories [14], or exploit geometrically exact approaches [15]. The latter are usually based on directed continuum models [16] or exploit asymptotic methods [17]. A number of reviews of such theories are available in the literature and summarize the modelling approaches and complicating effects. Many theories, for example, have been developed for rotor blades with an initial twist [18]. In this regard, a wide-ranging review on pre-twisted rods has been proposed by Rosen [19], who covers several aspects of the problem, from re-

sponse to static loads, to dynamics and stability issues. Kunz [20] has provided an overview of modelling methods for rotating beams, discussing how engineering theories for rotor blades have evolved over the years, from recognition of the importance of bending flexibility, to the development of linear equations for bending and torsion, to the introduction of nonlinear terms to such equations. A recent review on vibration issues in rotating beams summarizes beam theories and complicating effects, such as non-uniform cross-sections, initial curvature, twist and sweep [21]. In general, apart from pre-twisted rods, it seems that the results published for beam-like structures with initial taper and sweep are quite scarce, although all the mentioned geometric features may play an important role. This is especially true for modern blades, which are ever more flexible and longer than in the past, are pre-twisted and, in addition, are characterized by significant chord variations, which means the cross-sections taper is expected to have a significant influence on the stress and strain fields in the structure.

To date much progress has been made to develop powerful theories for beam-like structures. However, complex non-prismatic cases still require further investigation. In general, the geometry of the reference and current states must be appropriately described. Curvature, twist and taper are important design features and should be explicitly included in the model. Moreover, the analysis should not be restricted to small displacements. The model should provide the stress and strain fields in the three-dimensional solid, be rigorous and application-oriented, and provide classical results when applied to prismatic cases. Following these guidelines, a mathematical model to simulate the mechanical behaviour of the aforementioned structures is proposed in this work, which also extends the results of a previous work (see, for example, [22]). Specifically, a modelling approach for non-prismatic beam-like structures, undergoing large deflections, 3D cross-sectional warping and small strain, is introduced in section 2. The focus is on the effects of important geometric features, such as the taper of the transverse cross-sections. In this regards, new analytical results for bi-tapered beam-like structures are presented in section 3. Finally, numerical examples are proposed in section 4, along with comparisons with results from nonlinear 3D-FEM simulations.

2 MECHANICAL MODEL

An important point in modelling structures in large displacements is the description of their motion [23-28]. Here, we consider a non-prismatic beam-like structure as a collection of deformable plane figures (the transverse cross-sections) along a suitable 3D curve (the reference centre-line). We assume that each point of each cross-section in the reference state moves to its position in the current state through a global rigid motion on which a local generic (warping) motion is superimposed. In this way, the cross-sectional deformation can be examined independently of the global motion of the centre-line. It is thus possible to consider the global motion to be large, while the local motion and the strain may be small.

2.1 Geometry, kinematics and strain measures

Let us begin by introducing two local triads of orthogonal unit vectors. The first is the reference local triad, b_i, in the reference state, with b_1 aligned to the tangent vector of the reference centre-line (Figure 1, left). This frame is a function of the reference arch-length, s, i.e. $b_i=b_i(s)$. The second local triad, a_i, is an image of b_i in the current state. It is a function of the arch-length, s, and time, t, that is, $a_i=a_i(s,t)$. In general, the orientation of a_i and b_i relative to a fixed rectangular frame, c_i, can be defined using two proper orthogonal tensor fields, A and B, respectively, as follows

$$a_i = Ac_i, \quad b_i = Bc_i \tag{1}$$

Figure 1 shows a schematic representation of the reference and current states of the structure in terms of centre-lines and cross-sections. A generic cross-section in the reference state is contained in the plane of b_2 and b_3. In the current state, it may not remain plane (i.e. un-warped) and may not belong to the plane of a_2 and a_3. In general, its (possibly warped) current state is attained by superimposing an additional (warping) motion to the position of the points of the un-warped cross-section (as in Figure 1, right).

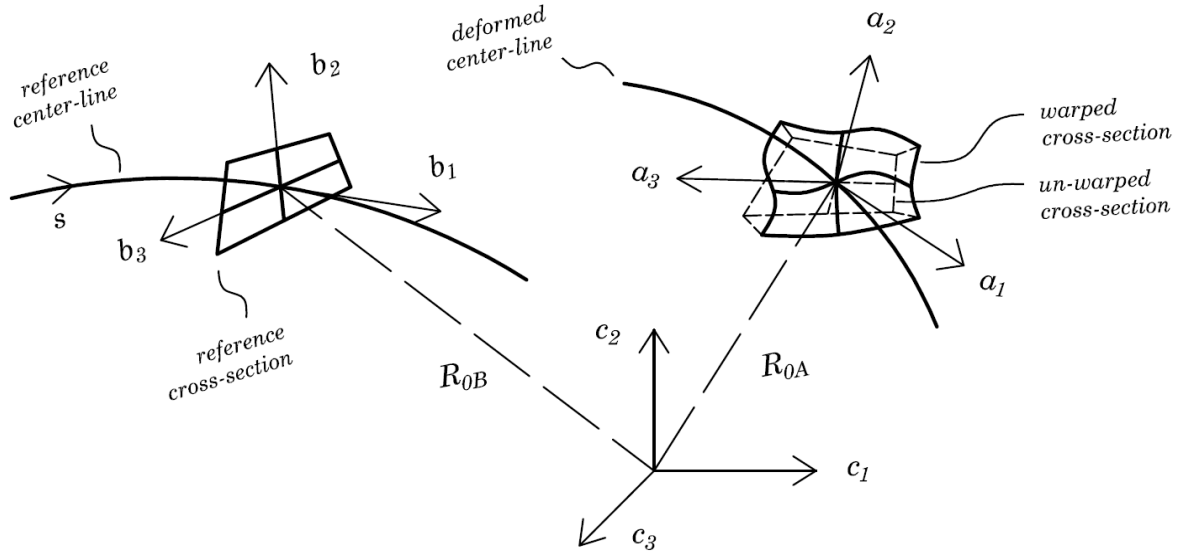

Figure 1: Representation of reference and current states in terms of centre-lines, cross-sections and local frames

We continue by introducing two mapping functions, R_A and R_B, to identify the position of the structure's points in the current and reference states, respectively. For the reference state, we define the (reference) mapping function

$$R_B(z_i) = R_{0B}(z_1) + x_\alpha(z_i) b_\alpha(z_1) \tag{2}$$

where R_{0B} is the position of the reference centre-line points relative to frame c_i, b_α are vectors of the reference local frame in the plane of the reference cross-section, x_α identify the position of the points in the reference cross-section relative to the reference centre-line, and, finally, z_i are three independent mathematical variables which do not depend on time. More precisely, z_1 is equal to arch-length s, while z_α belong to a bi-dimensional domain, referred to as Σ_0, which is used to map the position, x_α, of the cross-sections points.

Throughout this paper, Greek indices (α and β) take values 2 and 3, Latin indices (i, j and k) assume values 1, 2 and 3, and repeated indices are summed over their range.

It is worth noting that x_k may or may not be equal to z_k. The first option leads to common modelling approaches [8-10]. Here, we choose relations between x_k and z_k to explicitly simulate the shape of the considered non-prismatic structure. In particular, the span-wise variation in the shape of its cross-sections is modelled via the following map

$$x_i = \Lambda_{ij} z_j \tag{3}$$

where coefficients Λ_{ij} are functions of z_1. Hereafter, we consider curved and twisted beam-like structures with bi-tapered cross-sections, in which case map (3) reduces to

$$x_1 = z_1, \quad x_2 = z_2 \Lambda_2(z_1), \quad x_3 = z_3 \Lambda_3(z_1) \tag{4}$$

where coefficients Λ_α are functions of z_1.

The position of the structure's points in the current state are defined in a similar manner via the (current) mapping function

$$R_A(z_i,t) = R_{0A}(z_1,t) + x_\alpha(z_i)a_\alpha(z_1,t) + w_k(z_i,t)a_k(z_1,t) \tag{5}$$

where R_{0A} is a function mapping the position of the structure's centre-line points in the current state, while w_k are the components of 3D warping displacements in the local frame a_k, introduced to describe the geometry of the deformed state without a-priori approximations.

Now we introduce the kinematic variables we use to describe the structure's motion, starting with the orthogonal tensor field T, which defines the relative orientation between frames a_i and b_i, as follows

$$T = AB^T \tag{6}$$

Then we define two skew tensor fields, K_A and K_B, which are related to the curvature of the reference and current centre-lines of the structure, as follows

$$\begin{aligned} K_A &= A'A^T \\ K_B &= B'B^T \end{aligned} \tag{7}$$

The apex prime denotes the derivative with respect to arch-length s. By combining (6)-(7), the following identity holds

$$T^T T' = T^T K_A T - K_B \tag{8}$$

The left side of (8) defines a skew tensor field, herein denoted as K. The corresponding axial vector, k, can be determined via the relation

$$k = T^T k_A - k_B \tag{9}$$

where vector fields k_A and k_B are the axial vectors of the skew tensors K_A and K_B. These vectors are referred to here as curvature vectors in the current and reference states, respectively. It turns out that vector field k is the difference between the current curvature vector k_A, rotated back through tensor T, and reference curvature vector k_B. It thus contains information on the variation in curvature between the current and reference states.

In a similar manner, we introduce a vector field, γ, that is related to the difference between the current and reference centre-line tangent vectors, as follows

$$\gamma = T^T R'_{0A} - R'_{0B} \tag{10}$$

It can be shown that γ and k vanish for rigid motions and are invariant under superposed rigid motion [23-24]. Herein they are referred to as 1D strain measures.

We proceed by introducing the skew tensor field Ω, whose axial vector is called ω, which is associated with the variation in vectors a_i over time, t, as follows

$$\Omega = \dot{A}A^T \tag{11}$$

where the apex dot denotes derivative over time t.

The local triad b_i is independent of time, as is the function R_{0B}, which maps the positions of the centre-line's points in the reference state. On the contrary, function R_{0A} may change over time t. In particular, its variation is the time rate of change of the position of the current centre-line's points, v_0, that is

$$\dot{R}_{0A} = v_0 \tag{12}$$

By exploiting (6)-(12), we obtain the following kinematic relations

$$\begin{aligned} v_0' - \omega \wedge R_{0A}' &= T\gamma \\ \omega' &= Tk \end{aligned} \tag{13}$$

where the operator ∧ is the usual cross-product.

We are now in a position to introduce the tensor field, H, which is the gradient of the transformation between the reference and current states. It can be determined as follows

$$H = \frac{\partial R_A}{\partial R_B} = G_k \otimes g^k \tag{14}$$

In (14), G_k and g^k are covariant and contravariant base vectors in the current and reference states, respectively, and can be written in the form

$$\begin{aligned} g^1 &= g_0^{-1/2} b_1 \\ g^2 &= \Lambda_2^{-1}(b_2 - K_{B2\alpha}^* z_\alpha g_0^{-1/2} b_1) \\ g^3 &= \Lambda_3^{-1}(b_3 - K_{B3\alpha}^* z_\alpha g_0^{-1/2} b_1) \\ G_1 &= a_1 + \gamma_i a_i + K_{Ai\alpha}^* z_\alpha a_i + K_{Aij} w_j a_i + w_{i,1} a_i \\ G_2 &= \Lambda_2 a_2 + w_{i,2} a_i \\ G_3 &= \Lambda_3 a_3 + w_{i,3} a_i \end{aligned} \tag{15}$$

where

$$\begin{aligned} g_0^{1/2} &= 1 + K_{B1\alpha}^* z_\alpha \\ K_{(B\,or\,A)i\alpha}^* &= \Lambda_{i\alpha}' + \Lambda_{\beta\alpha} K_{(B\,or\,A)i\beta} \end{aligned} \tag{16}$$

When H is known, the Green-Lagrange strain tensor, *E*, can be calculated. In the following, we write tensor E in a form based on assumptions applicable to the considered structure. In particular, we introduce the characteristic dimension of the cross-sections, herein called *h*, the reference length of the centre-line, called *L*, and assume that *h* is much smaller than *L*. Moreover, we consider a thin structure and assume its centre-line curvatures are much smaller than *1/h*. Also, we assume the warping displacements, w_k, are small. More precisely, by introducing a non-dimensional parameter, ε, much smaller than one, they are considered to be of the same order as $h\varepsilon$, while the order of their derivative with respect to z_1 is $\varepsilon h/L$. In general, all deformation measures (i.e. the 1D strain measures γ and k, and 3D strain tensor E) are assumed to be small. In particular, their order of magnitude is at most ε.

For the considered structure, in the case of small strains and small local rotations, the strain tensor, *E*, can be determined via the following relation

$$E \approx \frac{T^T H + H^T T}{2} - I \tag{17}$$

2.2 Stress measures and constitutive model

Given the strain tensor, E, the choice of a constitutive model enables determining the corresponding stress fields as well [29]. Limiting our attention to elastic bodies in a purely mechanical theory, in the case of small strain, we use the following linear relation between the second Piola-Kirchhoff stress tensor, S, and the Green-Lagrange strain tensor, E,

$$S = 2\mu\, E + \lambda tr E\, I \tag{18}$$

where μ and λ are known scalar parameters related to Young's modulus and Poisson's ratio and I is the identity tensor [29]. For small strain and small local rotations, we also write

$$P = TS, \quad C = TST^T \tag{19}$$

where P is the first Piola-Kirchhoff stress tensor and C is the Cauchy stress tensor.

We are now in a position to define the stress resultants on each transverse cross-section of the beam-like structure. Using the first Piola-Kirchhoff stress tensor, P, for small warpings, small strains and small local rotations, we write

$$\begin{aligned} F &= T\int_{\Sigma} P_{i1} b_i \\ M &= T\int_{\Sigma} x_\alpha P_{i1}\, b_\alpha \wedge b_i \end{aligned} \tag{20}$$

In (20), Σ is the domain corresponding to the cross-section on which the integration is performed. The stress resultants are described in terms of two vector fields (i.e. the force F and moment M), which depends on the reference arch-length, s. Finally, the components of the first Piola-Kirchhoff stress tensor, P, are defined as follows

$$P_{ij} = P \cdot a_i \otimes b_j \tag{21}$$

By combining equations (14)-(20), the stress-resultants can be related to the geometric parameters of the structure and its 1D strain measures. However, such relations are actually known only if we know the warping fields, w_k. An approach to obtaining suitable warping functions is discussed in section 2.4.

2.3 Expended power and balance equations

To complete formulation of the model, we introduce the principle of expended power and the balance equations for the considered beam-like structure. For hyper-elastic bodies [29], we write the principle of expended power in the form

$$\int_A p \cdot v + \int_V b \cdot v = \frac{d}{dt}\int_V \Phi \tag{22}$$

In (22), *p* are surface loads per unit reference surface (A), *b* are body loads per unit reference volume (V), Φ is the 3D energy density function of the body, which is half the scalar product of the tensor fields S and E (i.e. 2Φ=S·E), and, finally, *v* is the time rate of change of the current position of the body's points, which is given by

$$v = v_0 + \omega \wedge x_\alpha a_\alpha + w^{\bullet} \tag{23}$$

where $w^{\bullet}$ is the time rate of change of the warping displacement.

For small warpings, strains, and local rotations, if the power expended by surface and body loads on the warping velocities is neglected, the external power, Π_e, reduces to the form

$$\Pi_e = \Delta\left(F \cdot v_0 + M \cdot \omega\right) + \int_s F_s \cdot v_0 + M_s \cdot \omega \tag{24}$$

where F_s and M_s are the resultants of the inertial actions and prescribed loads per unit length in the reference state, while symbol Δ simply indicates that the function between brackets is evaluated at both ends of the beam and the difference between the two values is taken.

It is worth noting that the 3D warping fields, w, may play an important role in determining the 3D energy density function, Φ, and are not neglected in the internal power, Π_i. However,

it is often useful to reduce the internal power, Π_i, in a common form for beam-like structures, by introducing a 1D energy density function, U, such that

$$\Pi_i = \frac{d}{dt}\int_s U \tag{25}$$

Note that if U depends only on the 1D strain measures (i.e. U(γ,k,s)), it is possible to write the principle of expended power for the considered structure in the form

$$\Delta\left(F \cdot v_0 + M \cdot \omega\right) + \int_s F_s \cdot v_0 + M_s \cdot \omega = \int_s f \cdot \gamma + m \cdot k \tag{26}$$

where the vector fields f and m are related to the vector fields F and M as follows

$$f = T^T F, \quad m = T^T M \tag{27}$$

and the force and moment, F and M, satisfy the following balance equations

$$\begin{aligned} F' + F_s &= 0 \\ M' + R'_{0A} \wedge F + M_s &= 0 \end{aligned} \tag{28}$$

At this point, we have the kinematic equations and strain measures, (9)-(13), the balance equations for the stress resultants, (28), and the principle of expended power for the considered beam-like structures, e.g. (26). We only need relations between the stress resultants and strain measures, which, in turn, depend on the warping fields. An approach to obtaining this result is discussed in the following section.

2.4 Cross-sections warping and centre-line deflection

In general, 3D nonlinear elasticity problems can be formulated as variational problems, but difficulties remain in directly solving such problems. However, for a beam-like structure with transverse dimensions much smaller than the longitudinal one, assumptions based on the smallness of the warping and strain fields can lead to useful simplifications. In particular, solving the 3D problem can be reduced to solution of two main problems [30]. One of the two problems governs the local distortion of the transverse cross-sections and is referred to here as the cross-section problem, the other governs the global deflection of the reference centre-line and is referred to here as the centre-line problem.

Hereafter, we consider the following variational statement to determine the warping fields responsible for cross-sectional deformation

$$\delta\int_V \Phi = 0 \tag{29}$$

In (29), the symbol δ stands for the variation operator, and the density function Φ depends on the warping fields, w_k. Warping fields satisfying (29) can be obtained via the corresponding Euler-Lagrange equations [31], by means of numerical methods, in general, or analytical approaches providing closed-form results, in particular cases. Once such problem is solved, we can also relate the stress resultants and 1D strain measures via equations (17)-(20).

That said, note that we also need the displacements of the structure's centre-line points to determine its current state. This result can be achieved by solving the centre-line problem, which is a non-linear problem governed by the kinematic, constitutive and balance equations introduced in section 2. Specifically, we are referring to the constitutive model introduced in section 2.2 (to relate the stress resultants and strain measures), and the balance equations in section 2.3 (for the stress resultants). The resulting set of (nonlinear) ordinary differential equations can then be numerically integrated with respect to arch-length s, using standard mathematical methods (see for example [32-33]).

In the following, we illustrate some analytical results (section 3) and numerical examples (section 4) obtainable through the proposed modelling approach.

3 ANALYTICAL RESULTS

The stress and strain fields in the considered structure can be determined through solution of (29). To this end, we exploit the aforementioned Euler-Lagrange equations, in which we maintain the terms up to the order εh/L. The result is that we obtain a mathematical problem, that is a partial differential equations (PDEs) problem, the solution of which enables determining the components of strain tensor E. Here, we also choose that the current local frames be tangent to the current centre-line and include possible shear deformations within the warping fields. In addition, in this section we focus on the effects of cross-sections' taper on the stress and strain fields and neglect those related to cross-sections' pre-twist.

Proceeding in this way, the components E_{11}, E_{21} and E_{31} of strain tensor E, which are related to the out-of-plane deformation of the cross-sections, can be written in the form

$$\begin{aligned} E_{11} &= k_2 x_3 - k_3 x_2 + \gamma_1 + e_{1,1} \\ 2E_{21} &= \Lambda_2^{-1} e_{1,2} - k_1 x_3 + 2(1+\nu)(k_2 x_3 - k_3 x_2 + \gamma_1)\Lambda_2^{-1}\Lambda_2' x_2 + e_2 \\ 2E_{31} &= \Lambda_3^{-1} e_{1,3} + k_1 x_2 + 2(1+\nu)(k_2 x_3 - k_3 x_2 + \gamma_1)\Lambda_3^{-1}\Lambda_3' x_3 + e_3 \end{aligned} \tag{30}$$

where the components of tensor E are defined by

$$E_{ij} = E \cdot b_i \otimes b_j \tag{31}$$

In (30), the subscript comma-α indicates the derivative with respect to z_α, comma-1 stands for the derivative over x_1, the scalar field e_1 is the solution to the following PDE problem

$$\begin{aligned} &\Lambda_2^{-2} e_{1,22} + \Lambda_3^{-2} e_{1,33} = 0 \quad in\ \Sigma_0 \\ &(e_{1,2} - \Lambda_2\Lambda_3 k_1 z_3) n_2 + (e_{1,3} - \Lambda_2\Lambda_3 k_1 z_3) n_3 = 0 \quad on\ \partial\Sigma_0 \end{aligned} \tag{32}$$

and, finally, the fields e_2 and e_3 can be obtained by solving the PDEs problem below

$$\begin{aligned} &\Lambda_2^{-1} e_{2,2} + \Lambda_3^{-1} e_{3,3} = \Lambda_2 a_2 z_2 + \Lambda_3 a_3 z_3 \quad in\ \Sigma_0 \\ &\Lambda_2^{-1} e_{3,2} - \Lambda_3^{-1} e_{2,3} = \Lambda_2 b_2 z_2 + \Lambda_3 b_3 z_3 \quad in\ \Sigma_0 \\ &\Lambda_2 e_2 n_2 + \Lambda_3 e_3 n_3 = 0 \quad on\ \partial\Sigma_0 \end{aligned} \tag{33}$$

In (33), coefficients a_α and b_α are linear functions of the 1D strain measures k_α and their first derivative with respect to s. Moreover, they explicitly depend on the initial shape of the structure through the taper coefficients, Λ_2 and Λ_3, as follows

$$\begin{aligned} a_2 &= +2(1+\nu)k_3' + 2(1+\nu)\left(\Lambda_3^{-1}\Lambda_3' + 2\Lambda_2^{-1}\Lambda_2'\right)k_3 \\ a_3 &= -2(1+\nu)k_2' - 2(1+\nu)\left(\Lambda_2^{-1}\Lambda_2' + 2\Lambda_3^{-1}\Lambda_3'\right)k_2 \\ b_2 &= -2\nu k_2' - 2(1+\nu)\Lambda_2^{-1}\Lambda_2' k_2 \\ b_3 &= -2\nu k_3' - 2(1+\nu)\Lambda_3^{-1}\Lambda_3' k_3 \end{aligned} \tag{34}$$

The approach used can also provide relations for components E_{22}, E_{33} and E_{23} of strain tensor E, which are related to cross-section in-plane deformations, plus an additional PDE problem in terms of unknown functions related to such in-plane deformations. In the following, we do not go into the details of the mathematical problem related to the in-plane deformations, but focus on the effects of taper included in functions e_1, e_2 and e_3, which have a significant influence on the strain and stress fields in non-prismatic beam-like structures.

3.1 The case of bi-tapered elliptical cross-sections

Let us now consider beam-like structures with bi-tapered elliptical cross-sections. For such a case we can provide analytical closed-form results, while for generic cross-section shapes problems (32)-(33) have to be solved via numerical methods (which is not surprising, given that analytical solutions are available only for a limited number of cases even in the classical linear theory of prismatic beams [5]).

In this case, the aforementioned PDEs problems can be solved without resorting to numerical methods. In particular, we obtain the following analytical results

$$\begin{aligned} e_1 &= (d_3^2 - \rho^{-2} d_2^2)(d_3^2 + \rho^{-2} d_2^2)^{-1} k_1 x_2 x_3 \\ e_2 &= +(c_2 x_2 + c_3 x_3) d_3^{-2} \Lambda_3^{-2} x_3 + (c_3 + a_2 d_2^2 \Lambda_2^2)(d_2^{-2} \Lambda_2^{-2} x_2^2 + d_3^{-2} \Lambda_3^{-2} x_3^2 - 1)/2 \\ e_3 &= -(c_2 x_2 + c_3 x_3) d_2^{-2} \Lambda_2^{-2} x_2 - (c_2 - a_3 d_3^2 \Lambda_3^2)(d_2^{-2} \Lambda_2^{-2} x_2^2 + d_3^{-2} \Lambda_3^{-2} x_3^2 - 1)/2 \end{aligned} \tag{35}$$

In (35), d_2 and d_3 are the major semi-axes of a reference elliptical cross-section (e.g. the one at the root section), while coefficients c_2 and c_3 are defined as follows

$$\begin{aligned} c_2 &= (b_2 + \rho^2 a_3)(1 + 3\rho^2)^{-1} \Lambda_3^2 d_3^2 \\ c_3 &= (b_3 - \rho^{-2} a_2)(1 + 3\rho^{-2})^{-1} \Lambda_2^2 d_2^2 \end{aligned} \tag{36}$$

where $\rho=\Lambda_3/\Lambda_2$ is a known function of z_1. Using this result, we can calculate the components of strain tensor (30), as well as the corresponding stress fields (18)-(19). An important result is that the effects of cross-sections' taper appear explicitly in all equations in terms of two specific application-oriented functions, that is, Λ_2 and Λ_3.

It is also worth noting that the model and analytical results presented here generalize the results of the classical linear theory of prismatic beams (see, for example, [34-35]), to which the present results reduce if the structure is prismatic and the centre-line deflection is small.

As already noted, analytical results such as those shown here (35) can only be obtained for a limited number of cases. However, problems (32)-(33) can always be solved with the aid of numerical methods for all other cases as well.

4 NUMERICAL EXAMPLES

In this section we show some quantitative results obtainable with the modelling approach presented in the previous sections, referred to as 3D-BLM in the following. To this end, we have implemented 3D-BLM in a numerical code in Matlab language and have exploited standard mathematical methods to numerically solve the corresponding differential equations [32-33]. The results obtained from 3D-BLM are then compared with those from 3D-FEM simulations performed with the commercial software Ansys, using a fine mesh and solid tetrahedral elements with 10 nodes and quadratic displacement behaviour [36].

In particular, test-case 1 addresses a rectangular cross-sectioned structure undergoing large displacements, while fixed at one end (the root) and loaded at the other (the tip) by a transverse force of progressively increasing magnitude (Figure 2). The results from 3D-BLM in terms of displacements and simulation times are compared to those from 3D-FEM to highlight the computational efficiency and accuracy of the proposed approach.

Test-case 2 is similar to test-case 1, except for its more complex geometry, which is curved, twisted and tapered already in the unstressed reference state (Figures 4). The goal of this second case is to show that the results obtainable for a simple geometry (e.g. test-case 1) can be achieved for more complex geometries as well.

Finally, the third and last test-case deals with a bi-tapered beam-like structure with elliptical cross-sections. The structure is fixed at the root and subjected to a flap-wise tip-force, F, as shown in Figure 9. The aim of this last test case is to illustrate the results obtainable with 3D-BLM in terms of 3D stress and strain fields as compared to those from 3D-FEM simulations. It also allows discussing the effects of cross-sections' taper, for which the corresponding analytical results have been presented in sections 3 and 3.1.

4.1 Test case 1

The first tests deal with a rectangular cross-sectioned structure undergoing large displacements while clamped at the root and loaded at the tip by a force, F, as in Figure 2. The structure's centre-line length is d_1=90m, while the cross-section dimensions are d_2=8m (edge-wise) and d_3=2m (flap-wise). The material properties are described in terms of reference values of Young's modulus, 70GPa, and Poisson's ratio, 0.25. Finally, the flap-wise tip-force, F, varies from 1000kN to 75000kN.

In all cases, the simulation time is significantly less than the time required by 3D-FEM simulations, while the accuracy of the results is almost the same. A summary of the results obtained in terms of tip-displacements and simulation times is shown in Figures 2 and 3.

Figures 2 (left) shows the un-deformed shape of the structure (F=0), the deformed shapes for F=10000kN, F=25000kN and F=50000kN, and the 3D-FEM deformed shape for F=25000kN (right), while Figure 3 provides comparisons between linear 3D-FEM, nonlinear 3D-FEM and 3D-BLM in terms of tip-displacements and simulation times.

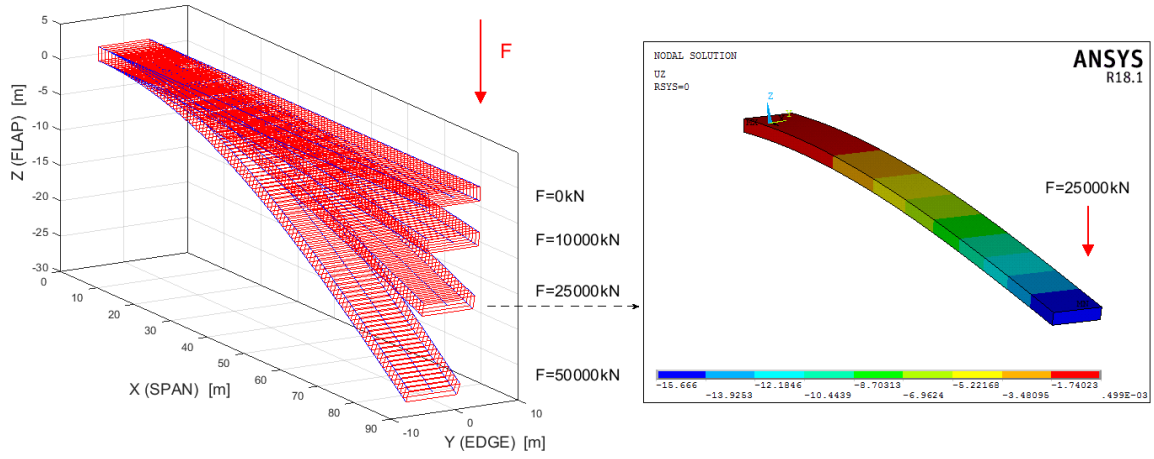

Figure 2: Global deflection with 3D-BLM for increasing F (left) and 3D-FEM for F=25000kN (right)

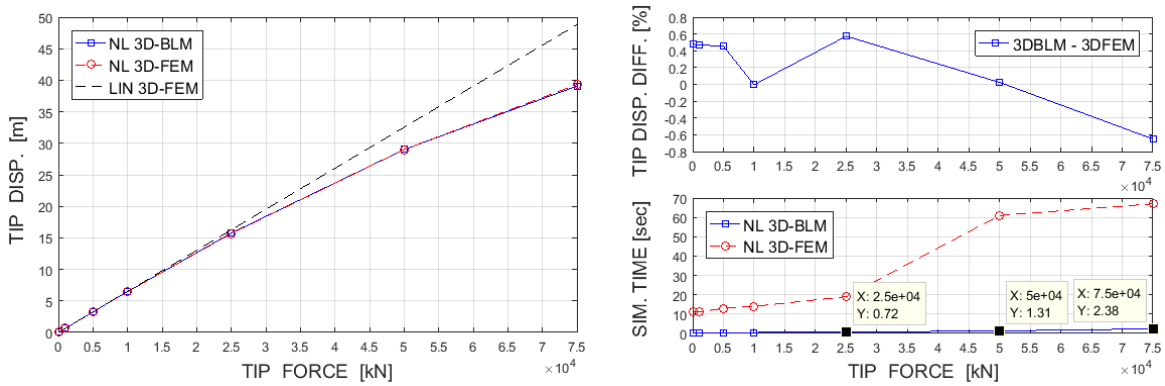

Figure 3: Comparison of tip-displacements (left), tip-displacement differences and simulation times (right)

4.2 Test case 2

The non-prismatic beam-like structure in this case is a pre-bent and swept beam, with constant curvatures and centre-line length of 90m (Figure 4). The reference local frames are pre-twisted (20deg/m). The major semi-axes of the reference elliptical cross-section at 18m from the root are d_2=2m (edge-wise) and d_3=0.5m (flap-wise). The sizes of the other cross-sections change according to the taper coefficients in Figure 4 (right). The material properties are summarized by reference values of Young's modulus, 70GPa, and Poisson's ratio, 0.25. Finally, the structure is clamped at the root and loaded at the tip by a flap-wise force, F, which varies from 100kN to 1000kN (as in Figure 5).

The results obtained in terms of tip-displacements and simulation times are summarized in Figure 6. As in test-case 1, the simulation times are significantly less than those required by nonlinear 3D-FEM analyses, while the accuracy of the results is once again nearly the same.

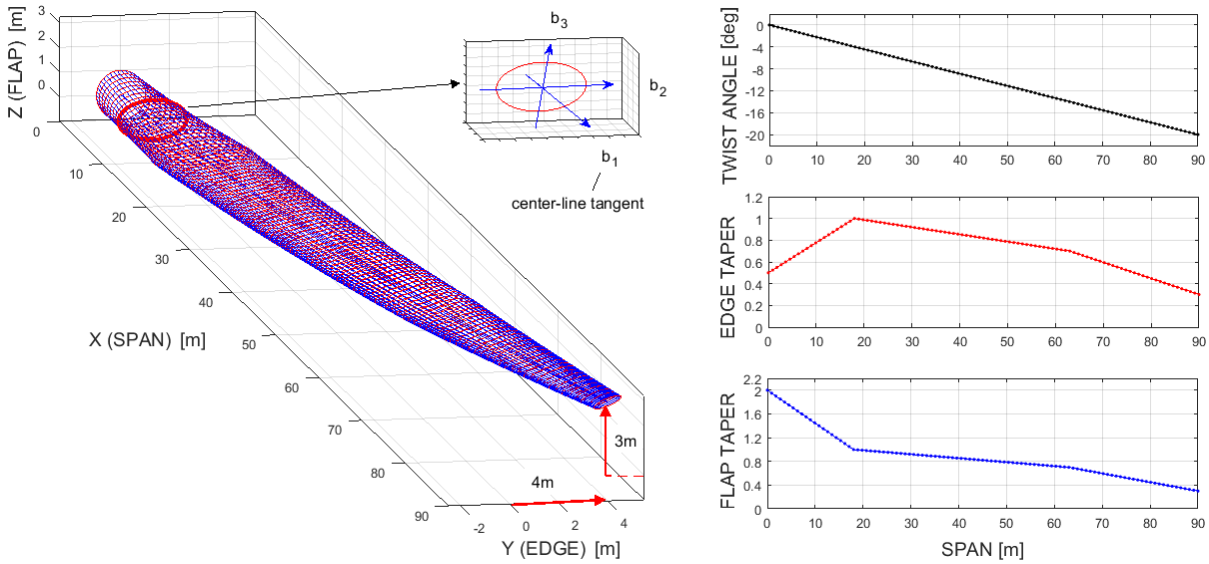

Figure 4: Curved, twisted and tapered beam-like structure (left), and its taper and twist coefficients (right)

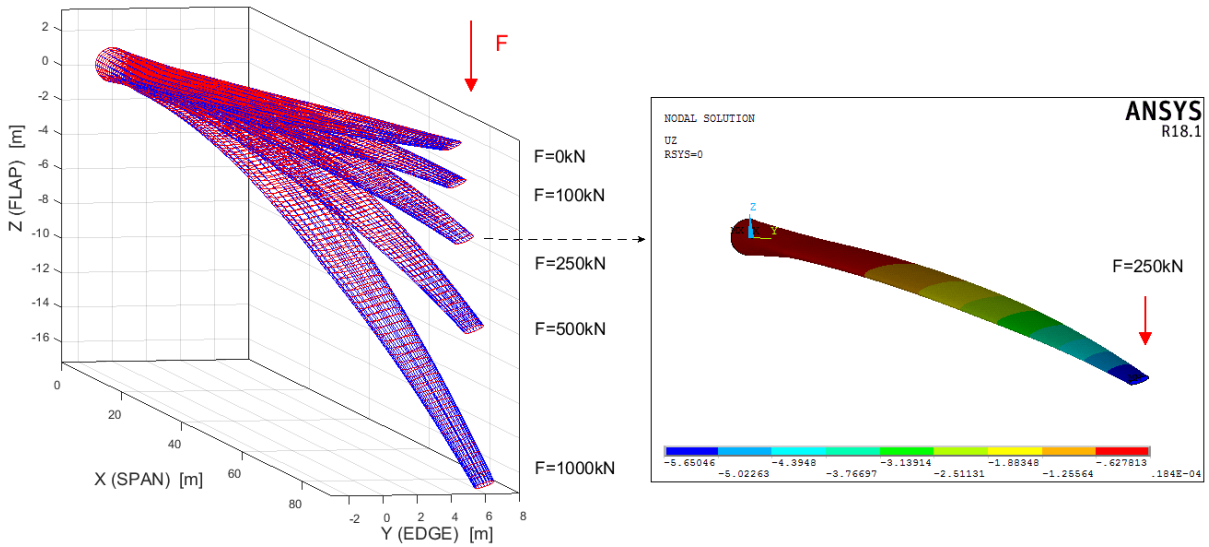

Figure 5: Global deflection using 3D-BLM for increasing F (left) and 3D-FEM for F=250kN (right)

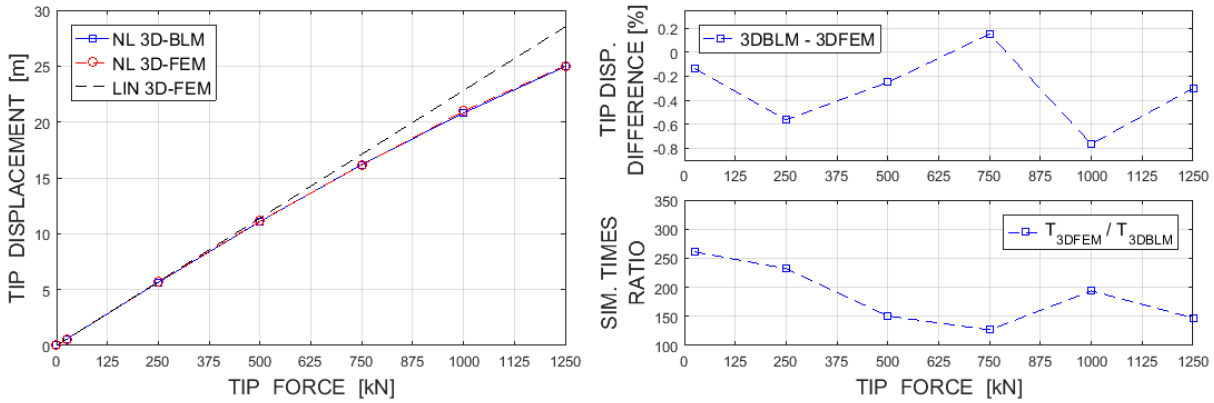

Figure 6: Comparison of tip-displacement (left), tip-displacement differences and simulation times (right)

Apart from those results, the model is able to provide other meaningful information, such as the displacements of the centre-line's points, the rotation of the local frames and the change in curvature of the beam-like structure, as well as the corresponding force and moments stress resultant with respect to the current local frames.

Figure 7, for example, shows the centre-line displacements for different tip-forces, while Figure 8 reports the local frames orientation in terms of Euler angles. We have considered the set of Euler angles corresponding to a first rotation, θ, about the initial z-axis, a second rotation, γ, about the intermediate y-axis, and a third rotation, ψ, about the final x-axis.

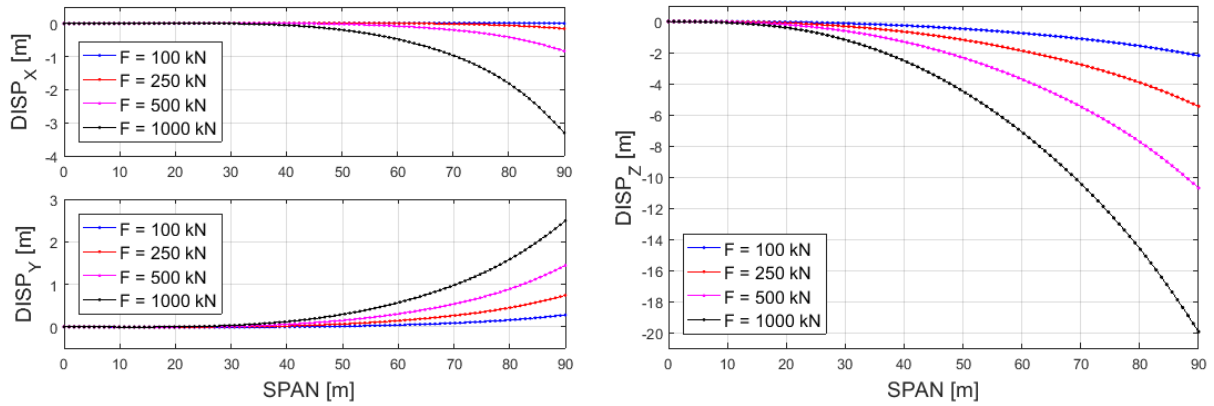

Figure 7: Displacement of the reference centre-line points using 3D-BLM for increasing F

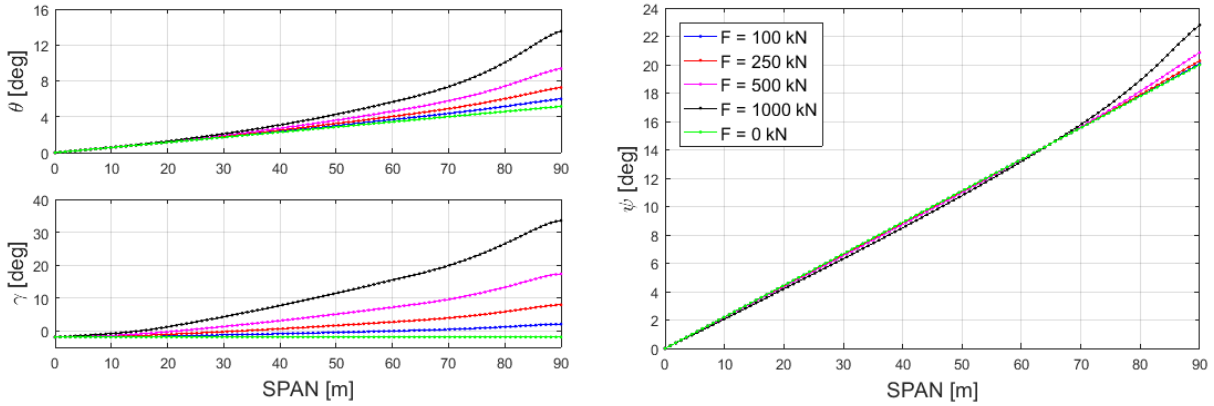

Figure 8: Local frames orientation in terms of Euler angles before (F=0) and after (F>0) deformation

4.3 Test case 3

The third and last test-case deals with a bi-tapered beam-like structure with elliptical cross-sections undergoing large deflections. The centre-line length is 100m. The major semi-axes at the root section are d_2=4m (edge-wise) and d_3=1m (flap-wise). The sizes of the other cross-sections decrease linearly from the root to the tip, with a reduction at the tip equal to 30% edge-wise and 15% flap-wise. The material properties are again described in terms of reference values of Young's modulus, 70GPa, and Poisson's ratio, 0.25. The structure is clamped at the root and loaded at the tip by a flap-wise force, F, as shown in Figure 9.

Also in this case we can obtain the same set of results as for the structures presented in the previous sections. Figure 9, for example, shows the un-deformed structure (F=0), its deformed shapes for F=1000kN, F=5000kN, and F=10000N (left), and comparisons with the results from 3D-FEM simulations in terms of centre-line displacements (right), while Figure 10 shows comparisons in terms of tip-displacements (left) and simulation times (right).

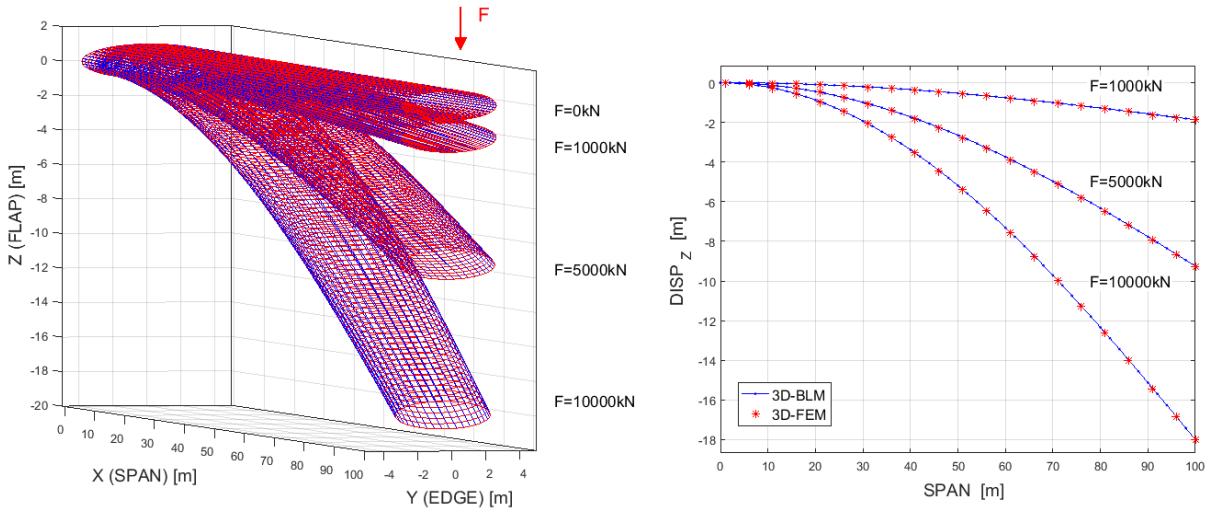

Figure 9: Bi-tapered structure deflection with 3D-BLM (left) and comparison with 3D-FEM (right)

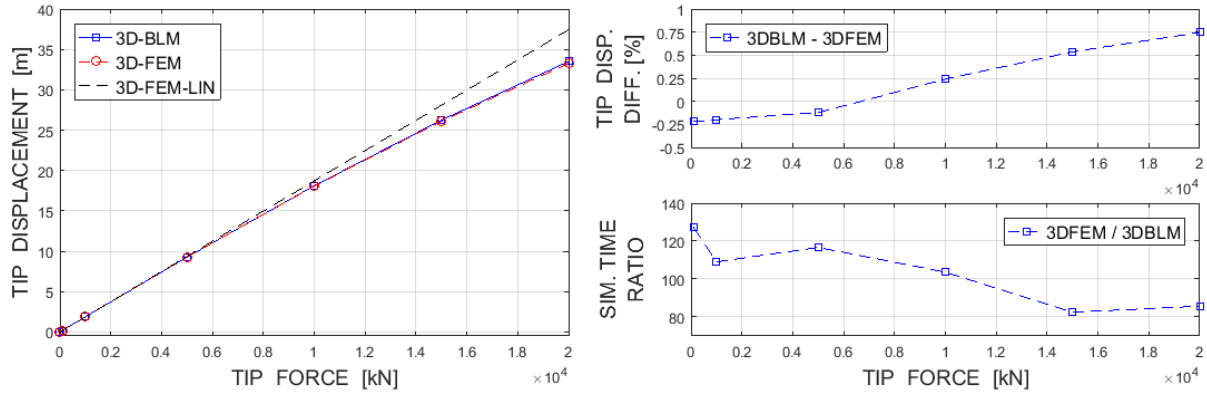

Figure 10: Comparison of tip-displacements (left), tip-displacement differences and simulation times (right)

Apart from such information, the model can provide useful results also in terms of stress and strain fields in the three-dimensional solid (see, for example, Figures 11-17).

We thus proceed by examining the results obtainable in terms of stress and strain fields for two values of tip-force, F, corresponding to small, F=1000kN, and large, F=15000kN, centre-line deflections. In doing so, we also highlight important effects of cross-sections' taper, for which the corresponding analytical results have been presented in section 3.

Concerning taper, one important effect is certainly related to span-wise variation in cross-section rigidities (such as bending rigidities), which affect centre-line deflection and, in turn, the stress and strain fields in the structure. This effect is directly accounted for through the taper functions, Λ_α, which act as scaling factors for the aforementioned rigidities [21].

A second important effect is instead related to span-wise variation in taper functions per unit centre-line length, or in other words, the derivative of such functions over arch-length s, Λ'_α. This latter directly affect the stress and strain fields in the three-dimensional solid, as also shown by equations (30)-(34). Figures 11 and 12, for example, show the importance of such effect in terms of component E_{31} of strain tensor E, for F=1000kN and F=15000kN, at three reference cross-sections (at 30%, 50% and 70% of the span-wise length). In particular, the results obtained from "full 3D-BLM" (blue lines), which includes all aforementioned taper effects, are compared to those obtained from "truncated 3D-BLM" (black lines), in which the effects related to the derivative of taper coefficients are neglected.

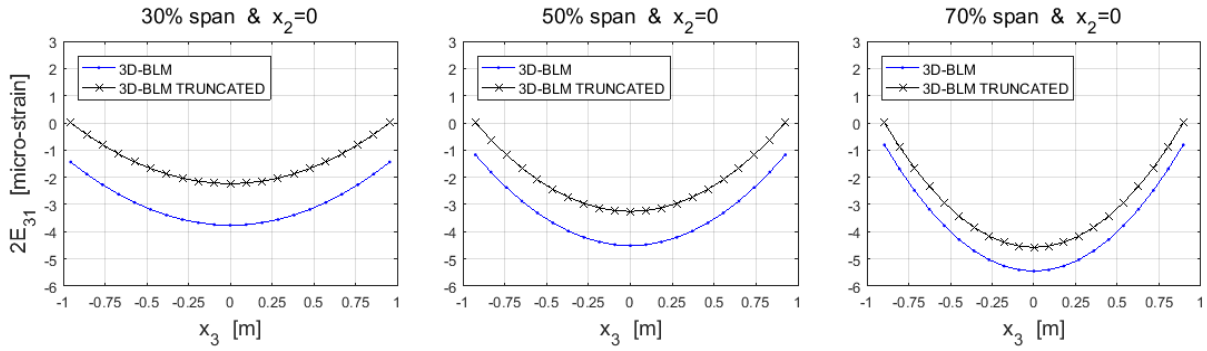

Figure 11: Effects of taper on $2E_{31}$ in the cross-sections at 30%, 50%, 70% span for F=1000kN

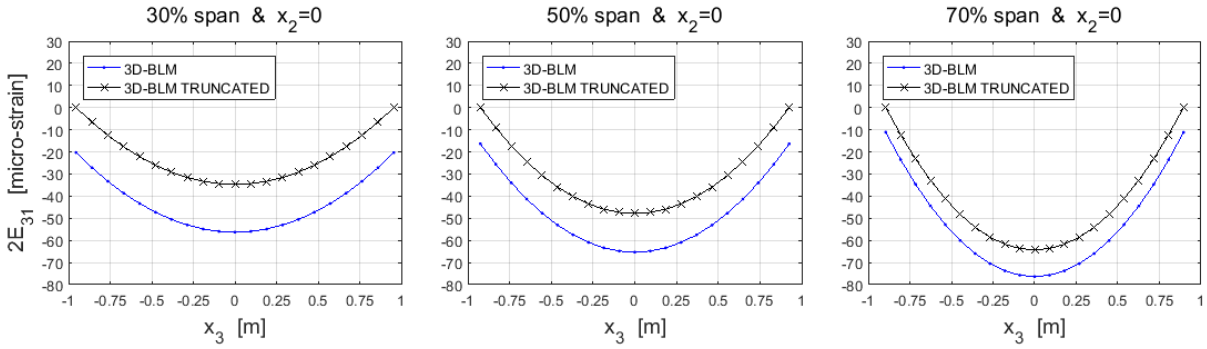

Figure 12: Effects of taper on $2E_{31}$ in the cross-sections at 30%, 50%, 70% span for F=15000kN

Finally, let us conclude by comparing the results obtained via 3D-BLM (full model) with those from 3D-FEM simulations in terms of the components of Cauchy stress tensor, C, for the same two values of tip-force, F=1000kN and F=15000kN.

In particular, Figures 13 and 14 show the results obtained for the longitudinal stress, C_{xx}, at three reference cross-sections, while Figures 15 and 16 present similar plots for the transverse shear stress, C_{zx}. Finally, Figure 17 provides the results in terms of span-wise variation in the maximum cross-sectional value of the longitudinal stress, max-C_{xx}, for F=1000kN (left) and F=15000kN (right).

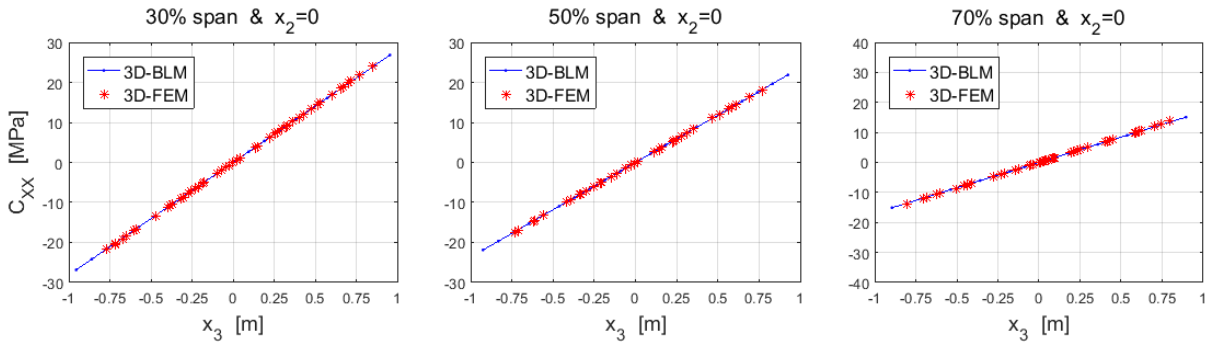

Figure 13: Longitudinal stress C_{XX} in the cross-sections at 30%, 50%, 70% span for F=1000kN

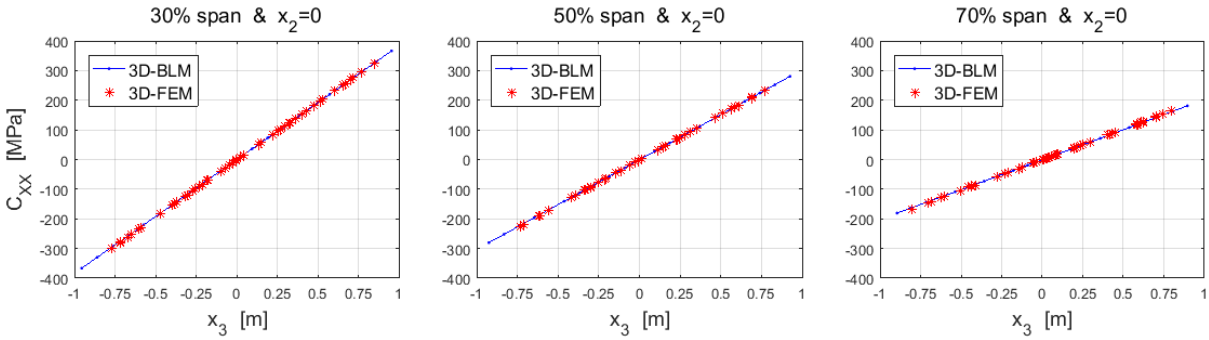

Figure 14: Longitudinal stress C_{XX} in the cross-sections at 30%, 50%, 70% span for F=15000kN

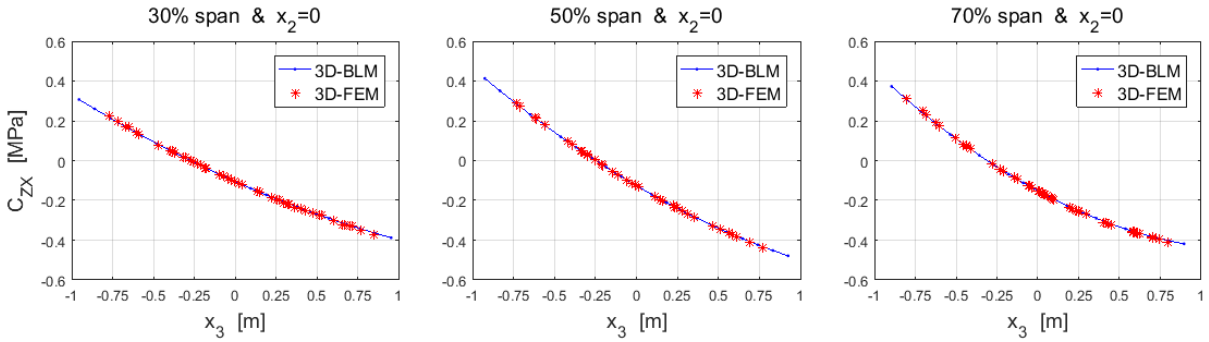

Figure 15: Transverse shear stress C_{ZX} in the cross-sections at 30%, 50%, 70% span for F=1000kN

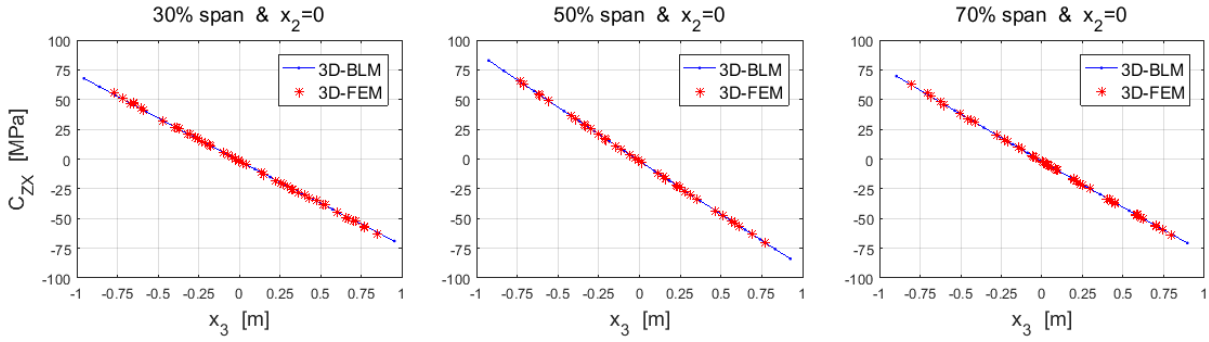

Figure 16: Transverse shear stress C_{ZX} in the cross-sections at 30%, 50%, 70% span for F=15000kN

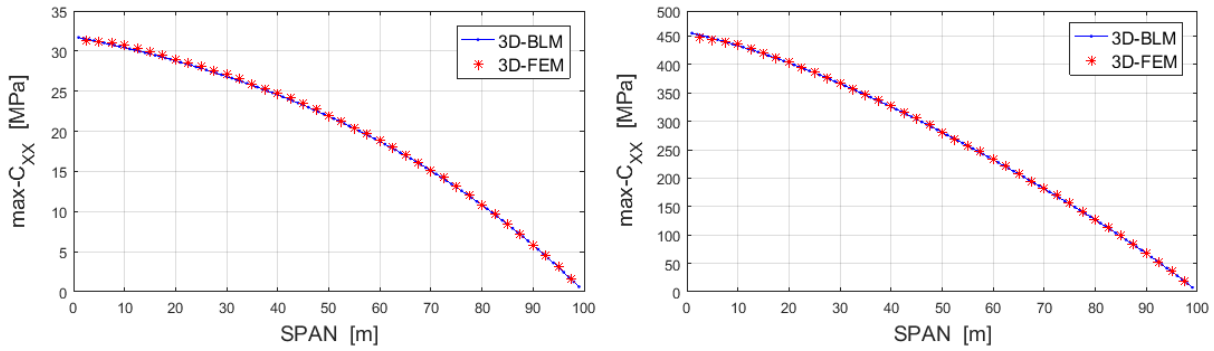

Figure 17: Span-wise variation in max longitudinal stress C_{XX} for F=1000kN (left) and F=15000kN (right)

As confirmed by many simulations and illustrated in the reported examples, the proposed modelling approach performs well in terms of computational efficiency and accuracy. It can moreover be used to predict the mechanical behaviour of non-prismatic beam-like structures undergoing large centre-line deflections, 3D cross-sectional warping and small strains, as it can provide useful and accurate information on the deformed states of such structures, e.g. the corresponding displacement, strain and stress fields.

5 CONCLUSIONS

Wind turbine and helicopter rotor blades, as well as many other engineering structures, can be considered non-prismatic beam-like structures which may undergo large centre-line deflection, in- and out-of-plane cross-sectional warping and small strain. Their mechanical behaviour can be simulated through suitable 3D beam models, which are computationally efficient, accurate and explicitly consider their main geometric design characteristics, such as the taper of their transverse cross-sections.

This paper has proposed a mathematical model for the aforementioned structures. Prediction of their mechanical behaviour has been reduced to solution of two main problems, one of which regards the local distortion of the transverse cross-sections, while the other governs the global deflection of the reference centre-line. A variational approach and the smallness of the warping and strain fields have been exploited to express the 3D stress and strain fields in terms of 1D strain measures, 3D warping functions and geometric parameters. The proposed modelling approach has allowed us to obtain analytical results which represent a generalization of the results of the classical linear theory of prismatic beams to which the results presented reduce if the structure is prismatic and the centre-line deflection is small. The resulting model can moreover be implemented in an accurate, computationally efficient numerical code, as demonstrated through several numerical examples and comparisons with the results from nonlinear 3D-FEM simulations.

The analytical results presented herein regard cases in which the effects of cross-section pre-twist on the stress and strain fields are negligible. The inclusion of additional terms related to pre-twist (along with those already accounting for the effects of taper) may be important to accurately predict the stress and strain fields in a more general case. This is an important point for further investigation and will be the subject of a subsequent work. It would also be interesting to performing comparative analyses with other structural modelling approaches (other than 3D-FEM), in order to gauge the performance of different models for non-prismatic beam-like structures in terms of the information each approach can furnish directly (e.g. centre-line displacements, 1D strain measures, 3D stress and strain fields), as well as their computational efficiency and accuracy of results.

REFERENCES

[1] Ashwill T.D., Kanaby G., et al, Development of the swept twist adaptive rotor (STAR) blade, *48th AIAA Aerospace sciences meeting*, Orlando, FL, Jan. 4-7, 2010.

[2] Wang L., Liu X., Kolios A., State of the art in the aeroelasticity of wind turbine blades: aeroelastic modelling, *Renewable and sustainable energy review*, **64**, 195-210, 2016.

[3] Tanuma T., *Advances in steam turbines for modern power plants*, Woodhead Publishing, 1st ed., Sawston, Cambridge, UK, 2016.

[4] Althoff M., Patil M.J., Traugott J.P., Nonlinear modelling and control design of active helicopter blades, *Journal of the American Helicopter Society*, 57, 1-11, 2012.

[5] Love A.E.H., *A treatise on the mathematical theory of elasticity*, 4th ed., Dover Publications, NY, 1944.

[6] Reissner E., On finite deformation of space curved beams, *Journal of applied mathematics and physics*, **32**, 734-744, 1981.

[7] Antman S.S., Warner W.H., Dynamical theory of hyper-elastic rods, *Arch. Rational Mech. Anal.*, **23**, 135-162, 1966.

[8] Simo J.C., A finite strain beam formulation, the three-dimensional dynamic problem, part I, *Computer methods in applied mechanics and engineering*, **49**, 55-70, 1985.

[9] Yu W., Hodges D.H., Ho J.C., Variational asymptotic beam-sectional analysis - an updated version, *International journal of engineering science*, **59**, 40-64, 2012.

[10] Pai P.F., Three kinematic representations for modelling of high flexible beams and their applications, *International Journal of solids and structures*, **48**, 2764-2777, 2011.

[11] Rafiee M., Nitzsche F., Labrosse M.R., Rotating nanocomposite thin-walled beams undergoing large deformation, *Composite Structures*, **150**, 191-199, 2016.

[12] Rafiee M., Nitzsche F., Labrosse M.R., Cross-sectional design and analysis of multiscale carbon nanotubes-reinforced composite beams and blades, *International Journal of Applied Mechanics*, **10**, 2018.

[13] Migliaccio G., Ruta G, et al., Curved and twisted beam models for aeroelastic analysis of wind turbine blades in large displacements, *Proc. of XXIV AIMETA conference 2019, Lecture notes in mechanical engineering, Springer*, Cham, Switzerland, 2020.

[14] Rosen A., Friedmann P.P., Non linear equations of equilibrium for elastic helicopter or wind turbine blades undergoing moderate deformation, *NASA, CR-159478*, 1978.

[15] Hodges D.H., *Geometrically exact equations for beams, Encyclopedia of Continuum Mechanics, Springer Verlag*, Germany, 2018.

[16] Rubin M.B., Cosserat theories: shells, rods and points, *Solid mechanics and its applications*, Springer Netherlands, 1st ed., 2000.

[17] Atilgan A.R., Hodges D.H., et al, Application of the variational asymptotic method to static and dynamic behavior of elastic beams, *AIAA Journal*, 91-1026-CP, 1991.

[18] Hodges D.H., Review of composite rotor blades modeling, *AIAA Journal*, **28**, 561-565, 1990.

[19] Rosen A., Structural and dynamic behavior of pre-twisted rods and beams, *American Society of Mechanical Engineers*, **44**, 483-515, 1991.

[20] Kunz D.L., Survey and comparison of engineering beam theories for helicopter rotor blades, *Journal of Aircraft*, **31**, 473-479, 1994.

[21] Rafiee M., Nitzsche F., Labrosse M., Dynamics, vibration and control of rotating composite beams and blades: a critical review, *Thin-walled structures*, **119**, 795-819, 2017.

[22] Migliaccio G., Ruta G., et al., Beamlike models for the analyses of curved, twisted and tapered horizontal-axis wind turbine (HAWT) blades undergoing large displacements, *Wind Energ. Sci.*, **5**, 685-698, https://doi.org/10.5194/wes-5-685-2020, 2020.

[23] Ibrahimbegovic A., On finite element implementation of geometrically nonlinear Reissner's beam theory: three-dimensional curved beam elements, *Computer methods in applied mechanics and engineering*, **122**, 11-26, 1995.

[24] Ruta G., Pignataro M., Rizzi N., A direct one-dimensional beam model for the flexural-torsional buckling of thin-walled beams, *Journal of Mechanics of materials and structures*, **1**, 1479-1496, 2006.

[25] Danielson D.A., Hodges D.H., Nonlinear beam kinematics by decomposition of the rotation tensor, *Journal of applied mechanics*, **54**, 258-262, 1987.

[26] Pai P.F., Three kinematic representations for modeling of high flexible beams and their applications, *International Journal of solids and structures*, **48**, 2764-2777, 2011

[27] Argyris J., An excursion into large rotations, *Computer methods in applied mechanics and engineering*, **32**, 85-155, 1982.

[28] Pai P.F., Problem in geometrically exact modeling of highly flexible beams, *Thin-walled structures*, **76**, 65-76, 2014.

[29] Gurtin M.E., *An introduction to continuum mechanics, Mathematics in science and engineering*, Academic Press, 1st ed., Sand Diego, California, USA, 1981.

[30] Berdichevsky V.L., On the energy of an elastic rod, *Journal of Applied Mathematics and Mechanics*, **45**, 518-529, 1981.

[31] Courant R., Hilbert D., *Methods of mathematical physics*, Interscience Publisher, 1st ed., New York, USA, 1953.

[32] Zwillinger D., *Handbook of differential equations*, Academic Press, San Diego, 1992.

[33] Ascher U.M., Mattheij R.M., Russel R.D., *Numerical solution of boundary value problems for ordinary differential equations*, Prentice-Hall, Inc., New Jersey, 1988.

[34] Sokolnikoff I.S., *Mathematical theory of elasticity*, McGraw-Hill Inc., 1st ed., New York, USA, 1946.

[35] Timoshenko S., Goodier J.N., *Theory of elasticity*, McGraw-Hill Inc., 2nd ed., New York, USA, 1951.

[36] Madenci E., Guven I., *The finite element method and applications in engineering using Ansys*, 2nd ed., Springer, New York, USA, 2015.